Hindawi
Journal of Electrical and Computer Engineering
Volume 2024, Article ID 8604095, 12 pages
https://doi.org/10.1155/2024/8604095

Research Article

Simulation Analysis of Arc-Quenching Performance of Eco-Friendly Insulating Gas Mixture of CF_3I and CO_2 under Impulse Arc

Dong Wu, Wengui Chen, and Zelin Ji

Key Laboratory of Advanced Manufacturing and Automation Technology, Guilin University of Technology, Education Department of Guangxi Zhuang Autonomous Region, Guilin 541006, China

Correspondence should be addressed to Dong Wu; wudong@glut.edu.cn

Received 1 October 2023; Revised 13 January 2024; Accepted 9 May 2024; Published 18 May 2024

Academic Editor: Prince Jain

Due to its superior insulating qualities, SF_6 gas is extensively used in the power sector. However, because of its poor environmental protection properties, finding ecologically acceptable insulating gas has become a critical challenge in the power sector in the context of pursuing green electricity. This work simulates the arc-quenching performance of a gas mixture of CF_3I and CO_2, which is thought to be a workable substitute for SF_6 gas. The COMSOL software is used to build a two-dimensional model of a single-pipe arc-quenching chamber based on the concepts of magnetohydrodynamics (MHD) theory. The lightning impulse current is made by applying electrical stimulation to pure CO_2 gas, gas mixtures with 10% CF_3I and 90% CO_2, and gas mixtures with 30% CF_3I and 70% CO_2 in the single-pipe arc-quenching chamber. During the first stage of arc formation, the results show that CF_3I/CO_2 gas mixtures with 10% and 30% CF_3I have lower electrical conductivity than pure CO_2 gas. An 8/20 μs lightning impulse current waveform with a magnitude of 4 kA is used for this observation. The highest airflow velocity for pure CO_2 is 1744 m/s, but the mixture of 10%/90% CF_3I/CO_2 has a maximum airflow velocity of 1593 m/s. The 30%/70% CF_3I/CO_2 mixture has the highest maximum airflow velocity at 1840 m/s. Airflow velocity increases and the overpressure in the arc-quenching chamber is prolonged when there is a greater concentration of CF_3I gas in the gas mixture. Consequently, these factors greatly reduce the duration of the arc-extinguishing time. The arc-quenching chamber's overpressure is extended when the amount of CF_3I gas in the gas mixture is increased, which increases the velocity of the airflow. As a result, these factors significantly decrease the duration of the arc-extinguishing time.

1. Introduction

Sulfur hexafluoride (SF_6) is a widely used gas with superior insulating qualities. However, its release into the atmosphere could be hazardous to the environment due to its lack of environmental precautions.

Under the terms of the 2016 Paris Agreement, all nations committed to achieving a complete cessation of greenhouse gas emissions by the year 2050 [1, 2]. During the 75th session of the General Assembly of the United Nations, China made a contribution to reducing the greenhouse effect and proposed to become carbon neutral by the year 2060 [3, 4]. Consequently, the necessity for an environmentally friendly insulating gas in the power sector is growing.

The range of ecologically friendly solutions has increased due to the recent upsurge in research on environmental insulating gases. The gases that are being studied are CF_3I, C_4F_7N, and c-C_4F_8 [5–8]. More environmentally acceptable insulating gases are available as a result of a new study on the subject that has surfaced in recent years. The gases that are being studied are c-C_4F_8, C_4F_7N, and CF_3I [9, 10].

CF_3I was formerly used as a refrigerant before its recognition as an insulating gas. It is currently thought to be a great alternative to conventional refrigerant components and "halon," a material used to battle fires [11]. CF_3I possesses halogen components with exceptional electron adsorption capabilities, thus increasing its insulating potency. Nevertheless, CF_3I has a notable liquefaction temperature of

−22.5°C when subjected to typical atmospheric conditions. To overcome this restriction, certain gases such as N_2 and CO_2 are added. CF_3I and its gas mixes have been thoroughly examined by both domestic and international experts to investigate their associated properties. Subjected to relatively nonuniform electric fields, research indicates that CF_3I has an insulating strength which is 1.2 times larger than SF_6. Both CF_3I and SF_6 gas demonstrate a significant loss in insulation capacity when exposed to extremely uneven electric fields, with CF_3I gas displaying a somewhat lower insulation capacity than SF6 gas. The insulating efficiency of the CF_3I/N_2 mixture can approach that of SF_6 under uniform electric fields, particularly for the 60/30% CF_3I/N_2 mixture [12]. The CF_3I/CO_2 mixture is tested on rod-plate, plate-plate, and coaxial cylindrical electrode, which demonstrates that the CF_3I mixture had superior insulation performance than SF_6 under lightning shock [13].

At present, most of the research on the insulation characteristics of CF_3I and its gas mixtures focuses on the breakdown characteristics and partial discharge characteristics of power frequency voltage [14, 15], but there are few studies on its breakdown characteristics under lightning impulse current. Based on this, the lightning protection gap's arc suppression structure for pressure explosion airflow pipes has been improved. Based on the Dalton law, this paper uses CF_3I/CO_2 mixing gas with different mixing ratios to replace the arc chamber gas and analyses changes in speed, pressure, and electrical conductivity in the arc pipe. The influence of various gas mixing ratios on the time required for arc extinguishment is investigated and analyzed. It lays the foundation for the realization of a new type of arc-extinguishing arrester.

2. Balance Theory of Arc Channel Energy

In a multichannel arc suppression arrangement, a shock arc is created when lightning strikes. Temperature and density abruptly shift as a result of the creation of a plasma in the gas due to a short current-carrying conduit. Shock waves are produced as the heat in the arc channel diffuses outward, increasing the arc channel's thickness and pressure in the process. The cylinder-shaped multipipe arc-extinguishing construction causes the gas to expand quickly to create a jet stream, and the arc is blasted longitudinally to increase arc deionization. The relationship between the energy balance of the discharge channels is studied to analyze the development process of the arc within the multipipe structure.

The shock wave overpressure is resolved using a cylindrical expansion model under the assumption that the arc cylinder channel is an ideal arc cylinder. The passage of gas in the arc channel complies with the laws of fluid dynamics, momentum conservation, and energy conservation. The overpressure produced by the high current impulse discharge arc when the impact wavefront is regarded as the arc border is [16]

$$\Delta P = K_1 \rho_0 u_p^2, \tag{1}$$

$$K_1 = \frac{2(\gamma + 1)}{(\gamma - 1)^2}, \tag{2}$$

where ρ_0 is the initial gas density, K_1 is the resistance coefficient of arc channel expansion, and u_p is the expansion speed of the arc channel, which can be simplified as a derivative of the arc channel radius.

The energy balance equation for the arc channel is [17–21] as follows:

$$M(t) + W(t) = E(t), \tag{3}$$

where E is the total energy of the arc channel, M is the energy by mechanical work, and W is the plasma energy.

Among these, the power injected into the arc channel by the high current impulse discharge can be integrated to determine the overall energy of the arc channel represented as

$$E(t) = \int_0^t \frac{i^2(\tau) l}{\sigma_a \pi r^2} d\tau, \tag{4}$$

where l is the length of the arc channel, σ_a is the arc conductivity, r is the radius of the arc channel, and $i(t)$ is the current of the arc channel.

In thermodynamics, W can be expressed as [17–21]

$$W(t) = \frac{P_1(t) V(t)}{\gamma - 1}, \tag{5}$$

where P_1 is the pressure of the arc channel, V is the volume of the arc channel, γ is the heat capacity ratio of the gas, and W is a constant value under the condition of an ideal gas.

The work performed by the expansion of the arc channel M is

$$M(t) = \int_0^{r_0} P_1(r) 2\pi r l dr. \tag{6}$$

By combining equations (1)–(6), it can be concluded that

$$\frac{2\pi^2 K_1 \rho_0 \sigma_a}{\gamma - 1} \left[r^4 \frac{dr}{dt} \frac{d^2 r}{dt^2} + \gamma \left(r \frac{dr}{dt} \right)^3 \right] = i^2. \tag{7}$$

The expression for the radius $r(t)$ obtained by organizing the above equation is

$$r(t) = \sqrt[6]{\frac{9}{\pi^2 K_1 \rho_0 \sigma_a}} \cdot \sqrt[3]{\int_0^t \sqrt{\int_0^{\tau'} i^2 d\tau} d\tau'}. \tag{8}$$

Given that arc current i is the lightning impulse current, it can be represented mathematically by a double exponential function, with the following model expression:

$$i(0, t) = I_m \left(e^{-\alpha t} - e^{-\beta t} \right), \tag{9}$$

where I_m is the current peak, α is the attenuation coefficient of the wavefront, and β is the attenuation coefficient of the wave tail. By combining equation (8), the expression for the variation of arc channel radius with time can be obtained as

$$r(t) = \left(\frac{9 I_m^2}{\pi^2 K_1 \rho_0 \sigma_a} \right)^{(1/6)} \cdot \left[\int_0^t \left(\int_0^{\tau'} \left(e^{-2\alpha\tau} - e^{-2\beta\tau} \right) d\tau \right)^{(1/2)} d\tau' \right]^{(1/3)}. \tag{10}$$

The equation above shows that the arc channel radius is influenced by the properties of the injection current, as well as the initial density and conductivity of the arc. The energy flowing through the channel amplifies as the maximum current amplifies, resulting in an increase in the radius of the arc channel. Then, taking into consideration the varying behaviors of the primary parameters of the various mixed gas ratios in the pipeline, equation (10) is modified to match the overpressure curve over time in equation (1).

The arc energy balance theory was used to fit the overpressure curve of a 10%CF_3I/90%CO_2 gas mixture with a starting pressure of 0.1 MPa and a room temperature inside the pipeline. This curve is depicted in Figure 1. As shown in Figure 1, it is obvious that the overall trend of the curve is decreasing. At $t = 1\,\mu$s, the overpressure is almost 31 MPa, and then the curve gradually decreases. Due to the internal pressure hysteresis in the simulation system, the pressure in the arc suppression pipeline did not reach its peak in a short period. The energy balance theory of arc channels only covers the early stages of arc channel formation. The edge of the extended curved channel continues to expand.

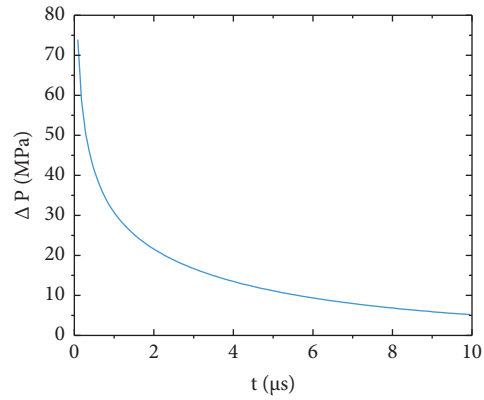

Figure 1: Overpressure attenuation curve of 10% CF_3I/90% CO_2 gas mixture.

3. Two-Dimensional Simulation Model of the Arc in the Arc-Quenching Chamber

When investigating its macroscopic motion, arc plasma is frequently viewed in magnetohydrodynamics as a conducting fluid, therefore the entire arc movement process and energy conversion must meet the Maxwell equation and Navier–Stokes equation. The conservation of mass, momentum, and energy are stated by the Navier–Stokes equations. The electromagnetic process is defined by the Maxwell equations, and the following hypotheses are put forth [22, 23]:

(1) Plasma is a hot plasma and meets the local thermodynamic equilibrium (LTE) condition.

(2) The injection current of the arc in the pipe is very high and the induced current is very negligible to it, which can be ignored.

(3) Arc moves fast in the environment of small pipe volume, assuming that it is the compressible fluid and flows along the smooth pipe.

(4) The effects of the Lorentz force, viscous dissipation of fluid motion, and viscous heating are ignored.

3.1. Governing Equations of MHD Mode. Arc plasma is typically a conductive fluid. Therefore, the energy characteristics and motion properties of the fluid must satisfy both Maxwell's equations and the Navier-Stokes equations. According to the theories mentioned above, the arc plasma follows the principles of mass, momentum, and energy conservation, as described by the Navier–Stokes equations. The electromagnetic phenomenon is mathematically defined by Maxwell's equations. The Navier–Stokes equations and Maxwell equations can be concurrently solved. The equation that governs the system is as follows:

(1) Mass conservation equation:

$$\frac{\partial \rho}{\partial \mathrm{t}} + \nabla \cdot (\rho \mathbf{v}) = 0. \tag{11}$$

(2) Energy balance equation:

$$\rho C_{\mathrm{p}} \left(\frac{\partial T}{\partial t} + \mathbf{v} \cdot \nabla T \right) - \nabla \cdot (k \nabla T) = Q, \tag{12}$$

$$Q = \frac{\partial}{\partial T} \left(\frac{5 k_B T}{2e} \right) (\nabla T \cdot J) + E \cdot J + Q_{rad}. \tag{13}$$

(3) Momentum conservation equation:

$$\rho \left(\frac{\partial \mathbf{v}}{\partial t} + \mathbf{v} \cdot \nabla \mathbf{v} \right) = \nabla \cdot \left[-pI + \mu \left(\nabla v + (\nabla v)^T \right) - \frac{2}{3} \mu (\nabla \cdot v) I \right] + F, \tag{14}$$

where the Lorentz force F is the volume force, and the Lorentz force considered here is as follows:

$$F = J \times B. \tag{15}$$

(4) Equation of state:

$$p = \rho R T. \tag{16}$$

(5) Current conservation equation:

$$\nabla \cdot (-\sigma \nabla \varphi) = 0. \tag{17}$$

(6) Poisson equation:

$$\mathbf{E} = -\nabla\varphi - \frac{\partial \mathbf{A}}{\partial t}. \quad (18)$$

(7) Ohm's law:

$$J = \sigma E. \quad (19)$$

(8) The magnetic field:

$$\nabla \times A = B, \quad (20)$$

where ρ is the density; v is the velocity vector; T is the temperature; C_p is the atmospheric heat capacity; k is the thermal conductivity; Q is the plasma heat source; k_B is Boltzmann's constant; e is the electron charge; J is the current density; Q_{rad} is the total volume radiation coefficient; p is the air pressure; I is the identity matrix; μ is the dynamic viscosity; F is the Lorentz force; B is the flux density of the self-induced magnetic field; R is the ideal gas constant; σ is the electrical conductivity; φ is the electric potential; E is the electric field intensity; and A is the magnetic vector potential.

3.2. Geometric Model and Boundary Conditions. With simultaneous consideration of the electromagnetic field, airflow field, and temperature field, a two-dimensional magnetofluid model of the arc is developed. In a multipipe arc-quenching chamber with a lightning impulse current, it primarily replicates arc discharge characteristics, airflow velocity, and pressure of CO_2 and CF_3I/CO_2 mixture gas containing 10% CF_3I gas and 30% CF_3I gas. The multichannel arc-extinguishing structure is used for the multichannel arc-extinguishing device at both ends of the insulator, as shown in Figure 2, where the design diagram of a single pipeline is shown in Figure 3.

Figure 3 shows one of the pipes in a multipipe arc-extinguishing structure. As a result of the symmetrical configuration of the single tube, a segment of it was selected for simulation study. The high-voltage electrode is labelled as B1 in the centre of Figure 3, and the grounding electrode is labelled as B3. Copper is the chosen material for the electrode, while electrical insulation is used on the other edges. The arc output is B4. B2 and B5 are set to be ceramics, and the corresponding gas is in the middle domain. The COMSOL software can be used to access the physical properties of copper and ceramics, and the literature can be used to locate the material properties of the gas combination [24].

The parameters of the mixed gas simulation are as follows. Figures 4(a)–4(d), respectively, represent the curves of mass density, heat capacity, viscosity coefficient, and thermal conductivity with temperature variation.

The following boundary conditions are established: the initial velocity is set at zero, and B1 is selected as the inlet. Based on the measurements from the previous experiment on the 10 kV line arrester shock coupling power frequency interrupting arc, the amplitude of the lightning surge current waveform at B1 is 4 kA with a duration of 8/20 μs. This waveform is applied to the high-voltage electrode. Figure 5 shows lightning shock current waveforms. The cathode is B3. B2 and B5 are thermal insulation walls. B2, B3, and B5 are antislip walls. The exit boundary of the airflow is set at B4, the pressure of which is one standard atmospheric pressure. In addition, the total simulation time is set at 88 μs, and the simulation step length is set to 4 μs.

4. Results and Analysis

In addition to the airflow velocity produced by the arc-quenching structure and the time it takes to reach that velocity, the gas employed affects the arc-extinguishing performance of the structure. Arc extinguishing is aided by the arc blowing toward the cathode, which speeds up the arc's cooling and dissociation. The arc is created in the arc-quenching structure to heat the gas, which causes the gas to expand and create a high-velocity airflow. The distinction in arc-extinguishing performance between CO_2 and CF_3I/CO_2 with different mixing ratios under lightning impulse current is observed in a multipipe arc-quenching chamber. When the lightning impulse current is applied, COMSOL's coupling iterative calculation for the MHD equation group is used to simulate how the conductivity, airflow velocity, pressure, and temperature are spread out in a single-pipe arc-quenching chamber.

(1) Conductivity distribution of different gases in a single-pipe arc-quenching chamber: The arc-quenching chamber's conductivity distributions for CO_2, 10%/90%CF_3I/CO_2, and 30%/70% CF_3I/CO_2 at various times are depicted in Figures 6–8, respectively. When lightning impulse current is delivered to the spherical gap at time $t = 4\,\mu$s, the arc conductivity of pure CO_2 is as illustrated in Figure 6(a). The CO_2 gas inside the arc-quenching structure is heated and expanded as the arc develops, flowing in the direction of the outlet. The arc is driven by the pressure burst airflow, which gradually develops from the two ball electrodes to the exit position with a trend towards moving to the exit. At this moment, conductivity is at its highest level of 1410 S/m.

The 10%/90% CF_3I/CO_2 gas mixture's conductivity distribution at $t = 4\,\mu$s is depicted in Figure 7(a). While the maximum value of conductivity is 924 S/m, which is lower than CO_2, the arc diameter is longer than pure CO_2 gas. At $t = 4\,\mu$s, the 30%/70% CF_3I/CO_2 gas mixture's conductivity distribution is depicted in Figure 8(a). The maximum conductivity is 846 S/m, which is lower than that of the 10%/90% CF_3I/CO_2, and the arc diameter is similar to that of the 10%/90% CF_3I/CO_2. At $t = 8\,\mu$s, Figure 6(b) demonstrates that the CO_2 arc conductivity's maximum value rises to 2400 S/m and the arc shifts in the direction of the outflow. The 10%/90% CF_3I/CO_2 arc conductivity rises to 1480 S/m in Figure 7(b). As indicated in Figure 8(b), the arc conductivity of 30%/70% CF_3I/CO_2 is 1610 S/m, but it moves more

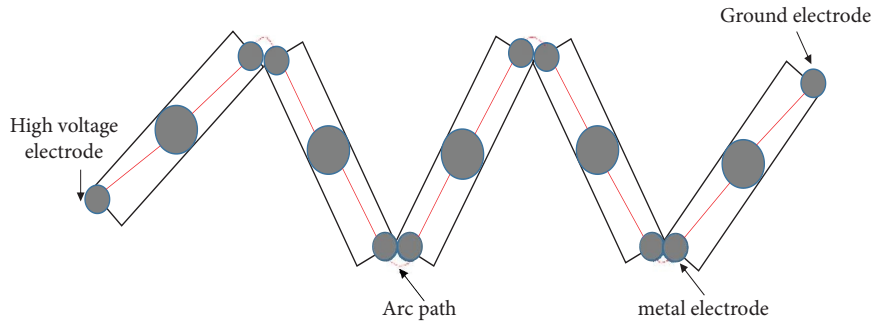

Figure 2: Design diagram of a multipipe arc-extinguishing structure.

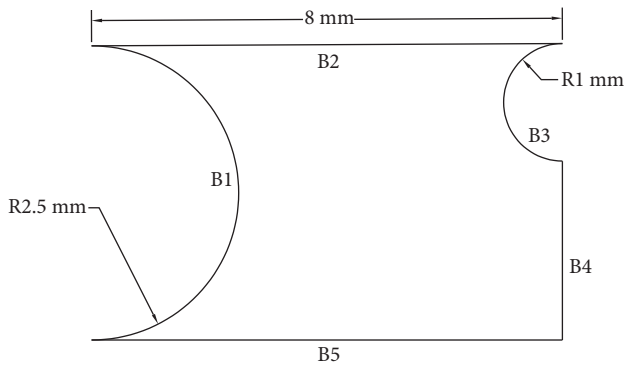

Figure 3: The geometry diagram of the arc-quenching structure.

in the direction of the exit than the arc of 10%/90% CF_3I/CO_2 gas combination. It is clear from the conductivity that 30%/70% CF_3I is more suited to putting out the arc.

(2) Curve of peak airflow of different gases in a single-pipe arc-quenching chamber: Figure 9 depicts the CO_2, 10%/90% CF_3I/CO_2, and 30%/70% CF_3I/CO_2 airflow velocity curves for the lightning impulse current. The airflow velocity shown on the graph represents the highest value attained at each instant. Each of the three curves rises quickly to the maximum airflow velocity before abruptly falling. The maximum airflow velocity of 10%/90% CF_3I/CO_2 is 1593 m/s, and the maximum airflow velocity of pure CO_2 is 1744 m/s at time $t = 4\,\mu$s. However, as the proportion of CF_3I in the CF_3I/CO_2 gas mixture increases, the maximum airflow velocity of 30%/70% CF_3I/CO_2 rises to 1840 m/s. It can be seen that the increase in the proportion of CF_3I contributes to the increase in airflow velocity, which strengthens the longitudinal blowing effect of the airflow on the arc. This is beneficial for quenching the arc. At $t = 8\,\mu$s, due to the greater value of arc conductivity of CO_2, the corresponding airflow velocity generated by the heated gas is greater compared to 10%/90% CF_3I/CO_2 and 30%/70% CF_3I/CO_2. However, after $t = 20\,\mu$s, the airflow rate of the gas mixture is always higher than that of the pure CO_2. Higher airflow speeds are conducive to accelerating the spread and release of the arc, extending the arc orbit, and speeding the arc extinguishment. Although the airflow velocity becomes smaller after $t = 12\,\mu$s and drops to a relatively low level, the arc has already dissipated most of its energy by accelerating the process of convective heat dissipation under the effect of high airflow. The gap of gas gradually restores the insulation strength, and the arc impedance increases, preventing the arc from reigniting.

(3) Pressure distribution of different gases in a multipipe arc-quenching chamber: under the lightning impulse current, the arc is generated rapidly in the arc-quenching chamber and then leads to the overpressure of shock. The CO_2 gas pressure distribution cloud charts are displayed in Figure 10. The pressure has a minimum value of 3.32×10^4 Pa and a maximum value of 1.05×10^5 Pa at time $t = 4\,\mu$s, indicating that the lightning impulse current has not yet reached its maximum value. However, based on the general cloud charts, the majority of the pressure is only at a low value. The values of air pressure as displayed in the overall air pressure cloud chart increase as the minimum value of the pressure increases to 7.74×10^4 Pa at $t = 8\,\mu$s. Evidently, the pressure at the outflow is higher than it was previously. The arc in the arc-quenching chamber heats the gas, which causes it to eject internally in the direction of the outlet and blow an arc.

Figure 11 shows the pressure distribution cloud charts for 10%/90% CF_3I/CO_2. Figure 10 shows that at time $t = 4\,\mu$s, the minimum pressure is 3.89×10^4 Pa and the maximum pressure is 1.12×10^5 Pa. Both figures exceed the figures for pure CO_2 gas. The values of pressure indicated in the overall pressure cloud chart increase as the minimum value of the pressure increases to 6.79×10^4 Pa at $t = 8\,\mu$s. Due to the strong Lorentz effect on fluids, which creates a higher pressure gradient in the centre of the single-pipe arc-quenching chamber, the pressure gradient gradually reduces as the gas is accelerated to flow.

Figure 12 shows the pressure distribution cloud charts of 30%/70% CF_3I/CO_2, which are similar to those of 10%/90% CF_3I/CO_2 at the beginning. At

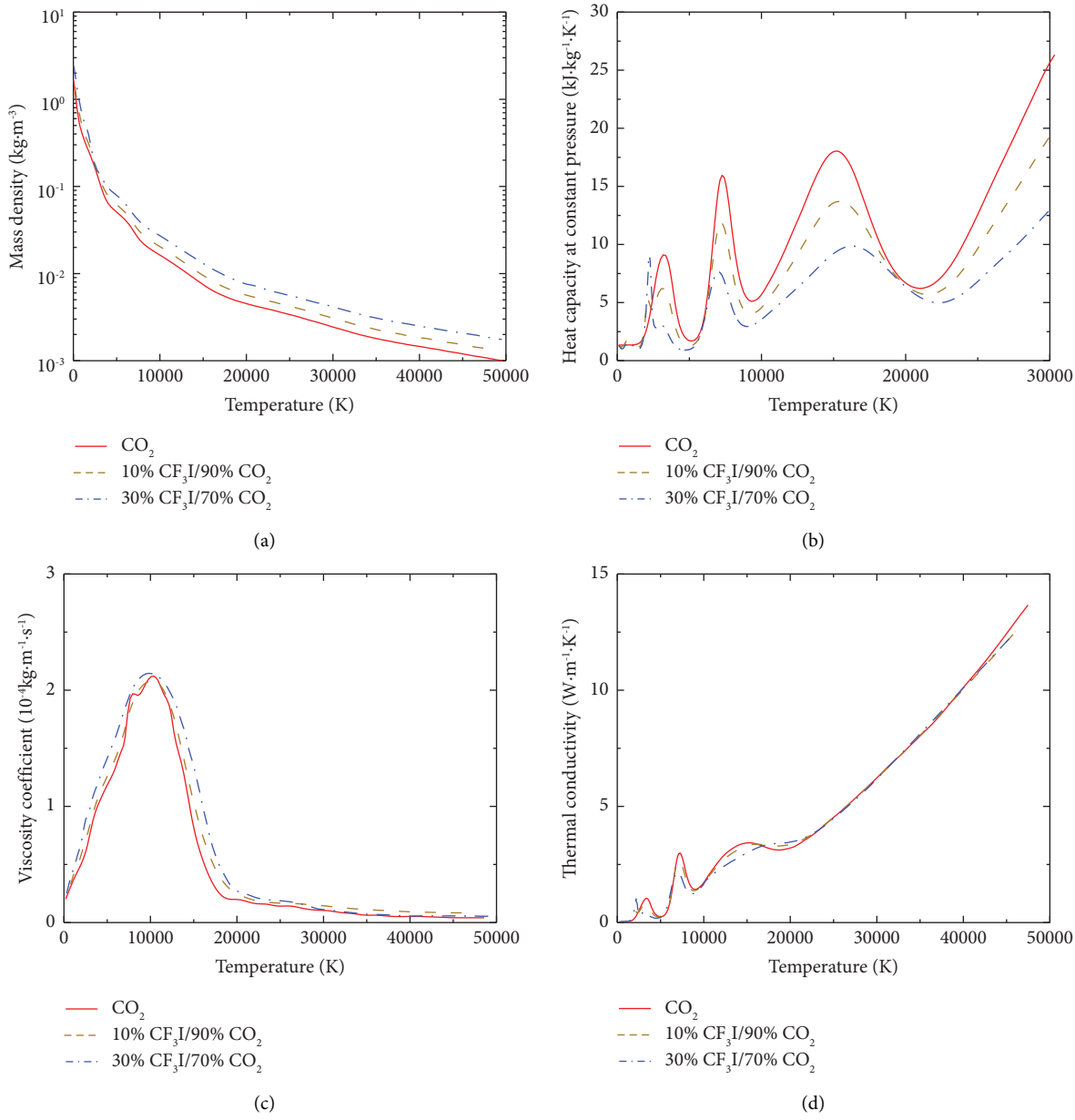

Figure 4: Mixed gas partial parameter diagram. (a) Mass density. (b) Heat capacity. (c) Viscosity coefficient. (d) Thermal conductivity.

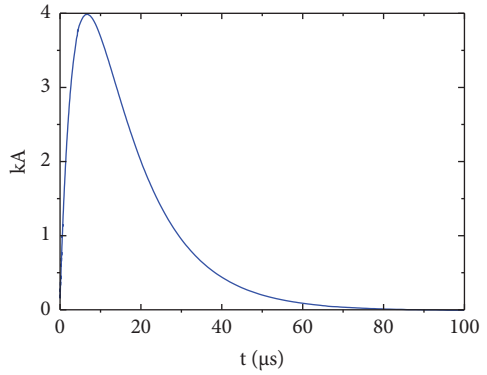

Figure 5: The waveform diagram of lightning current.

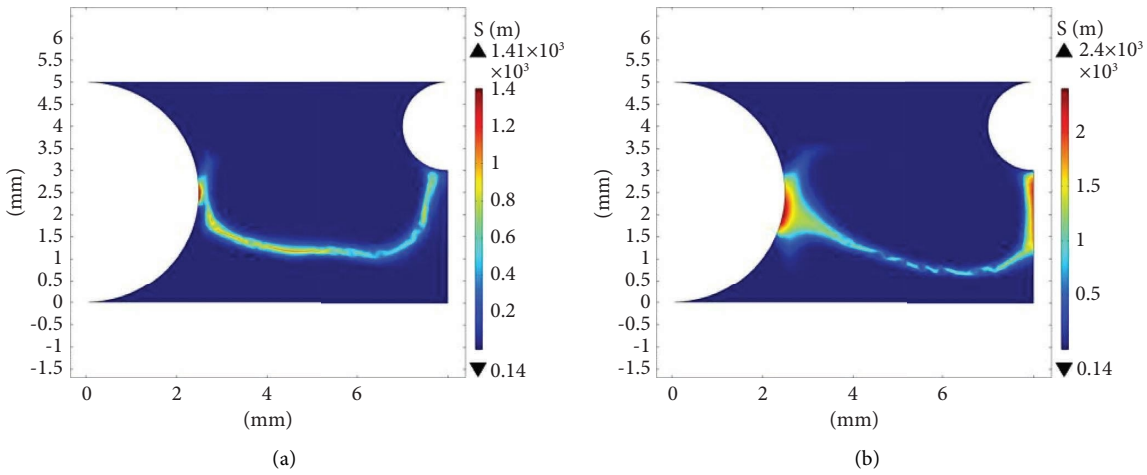

Figure 6: Conductivity distribution cloud charts of CO_2 under 4 kA lightning impulse current at different moments. (a) 4 μs. (b) 8 μs.

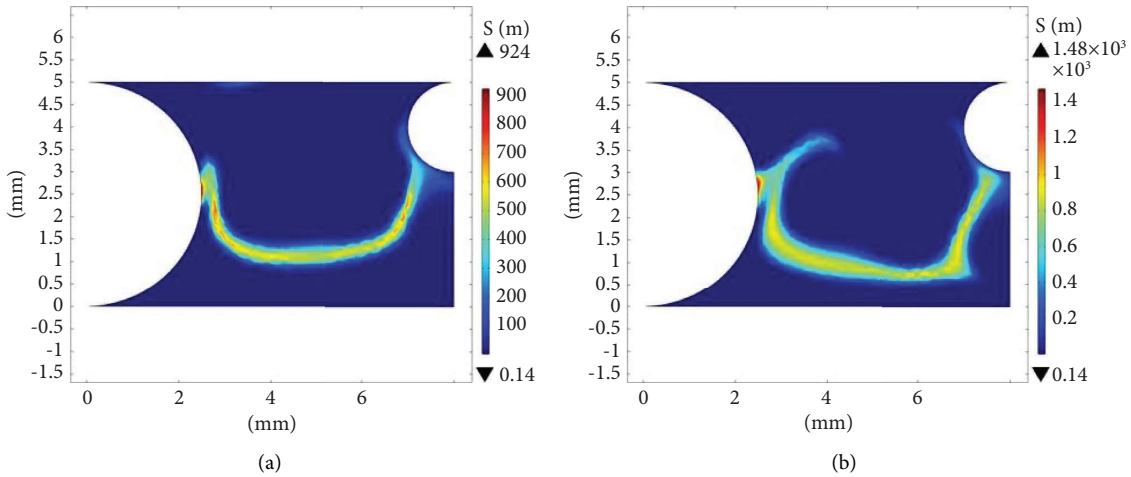

Figure 7: Conductivity distribution cloud charts of 10%/90% CF_3I/CO_2 under 4 kA lightning impulse current at different moments. (a) 4 μs. (b) 8 μs.

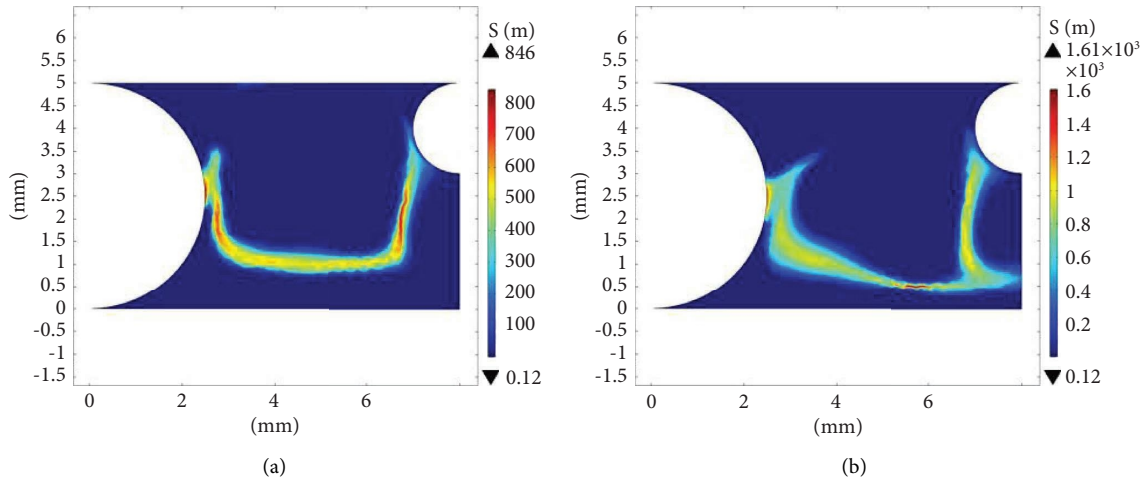

Figure 8: Electrical conductivity distribution cloud charts of 30%/70% CF_3I/CO_2 under 4 kA lightning impulse current at different moments. (a) 4 μs. (b) 8 μs.

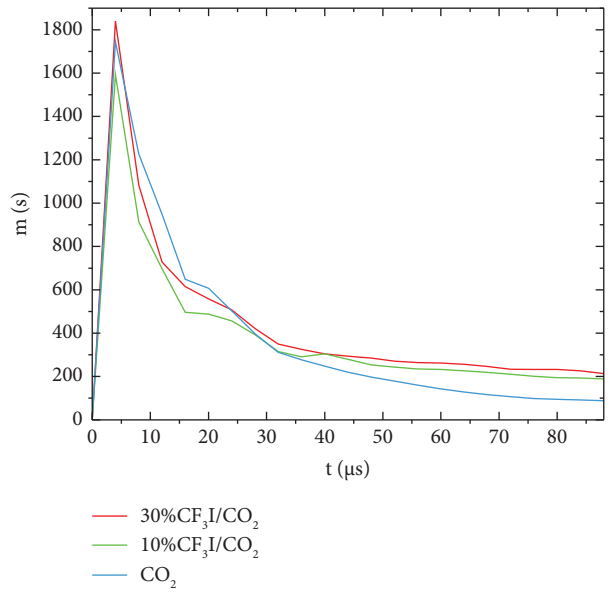

Figure 9: Curve of peak airflow in arc-quenching structure with simulation time.

$t = 12\,\mu s$, the overall pressure of CO_2 gas decreases, and the pressure is mainly concentrated at the outlet. At $t = 16\,\mu s$, the pressure of the middle part is close to the minimum value, indicating that the pressure decreases. However, from Figures 8 and 9, it can be seen that the overall pressure is still in a relatively high situation, from $t = 12\,\mu s$ to $t = 16\,\mu s$, indicating that the overpressure generated by the CF_3I gas mixture under the lightning impulse current lasts longer compared to the pure CO_2 gas. The longer-lasting effect on the arc is advantageous since it speeds up ion migration and arc extinguishment. According to the balance theory of arc channel energy, the more arc energy there is in the multipipe structure, the more pressure is produced by the accumulation in the pipe. When an arc forms, a shock wave overpressure is produced, which exerts pressure on the surrounding gas, expels the gas in the direction of the outlet, and creates a strong airflow velocity, all of which are essential for putting out the arc.

(4) Temperature distribution of different gases in a single-pipe arc-quenching chamber: at this point, the energy of the lightning current gradually transforms into the internal energy of the plasma and the energy of the arc channel expansion. According to the first section of the arc energy balance theory, the combustion of an arc belongs to the process of constantly changing energy, including the input of energy and the dissipation of energy. As time passes, the arc temperature reaches its maximum value, and due to the temperature difference, the mixed gas medium in the pipeline expands, resulting in a pressure explosion in the airflow. The shock wave energy inside the pipeline is converted by the energy of the arc channel, and the overpressure inside the pipeline can affect the changes in airflow velocity. As the energy of the arc gradually transforms into shock wave energy, the temperature of the arc gradually decreases. The temperature distribution cloud charts for several gases under a 4 kA lightning impulse current are shown in Figure 13 at $t = 88\,\mu s$. The temperature of CO_2 is 6801 K in Figure 13, whereas the temperatures of the 10%/90% CF_3I/CO_2 and 30%/70% CF_3I/CO_2 mixtures are 4741 K and 4822 K, respectively. This demonstrates that the CF_3I gas mixture quenches the arc more quickly than pure CO_2. The 10%/90% CF_3I/CO_2 has a wider and more concentrated area of higher temperatures, despite having a lower local maximum temperature than the 30%/70% CF_3I/CO_2.

(5) Simulation results: in light of the aforementioned data, it can be concluded that regardless of how the arc is generated or how it is ultimately extinguished, 30%/70% CF_3I/CO_2 gas performs better in terms of conductivity, airflow velocity, pressure, and temperature than 10%/90% CF_3I/CO_2 gas and pure CO_2 gas.

The arc-quenching structure mentioned above serves as the foundation for the simulation in this research. The ball-ball gap measures 4.5 mm, the radius of the right spherical electrode is 1 mm, and the left spherical electrode has a radius of 2.5 mm. In actuality, arc-quenching performance is influenced by the size and shape of various arc-quenching structures in addition to the differences in gases. Depending on the lightning current level and arc-quenching capacity needs, different-sized and shaped arc-quenching structures and types of complementary gases can be built to improve the arc-quenching performance.

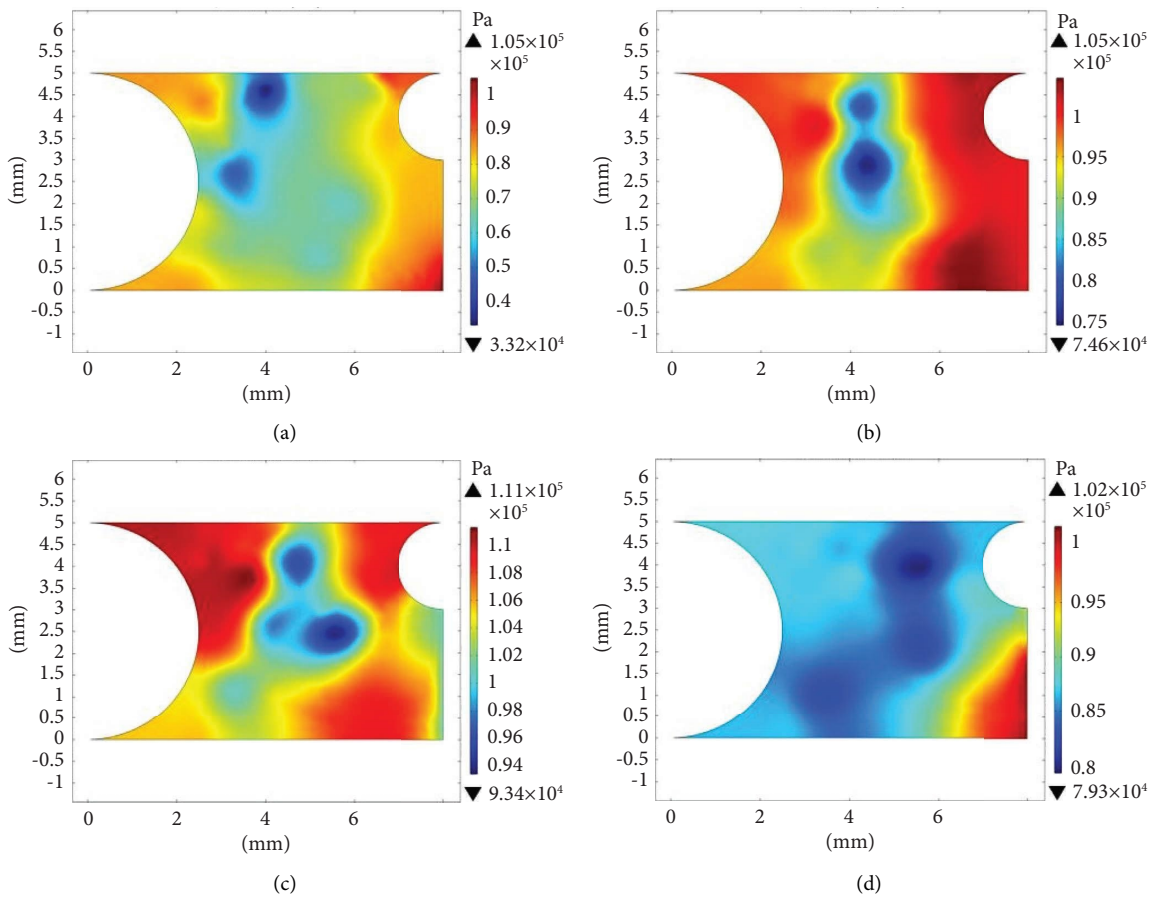

FIGURE 10: Pressure distribution cloud charts of CO_2 under 4 kA lightning impulse current at different times. (a) 4 μs. (b) 8 μs. (c) 12 μs. (d) 16 μs.

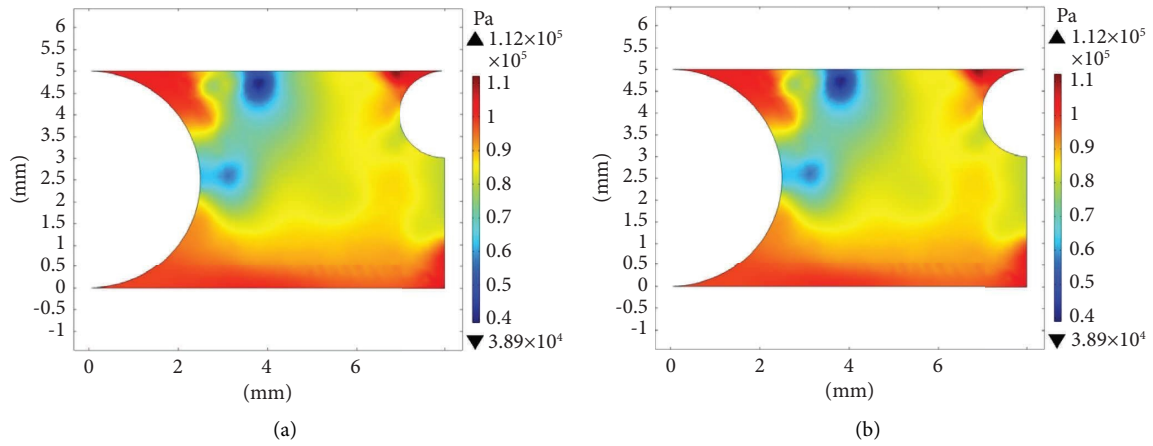

FIGURE 11: Continued.

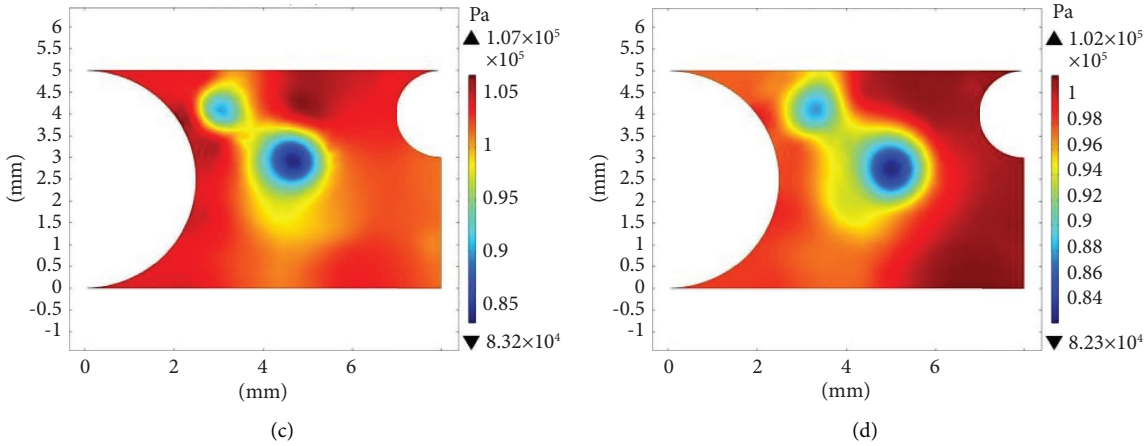

FIGURE 11: Pressure distribution cloud charts of 10%/90% CF_3I/CO_2 under 4 kA lightning impulse current at different times. (a) 4 μs. (b) 8 μs. (c) 12 μs (d) 16 μs.

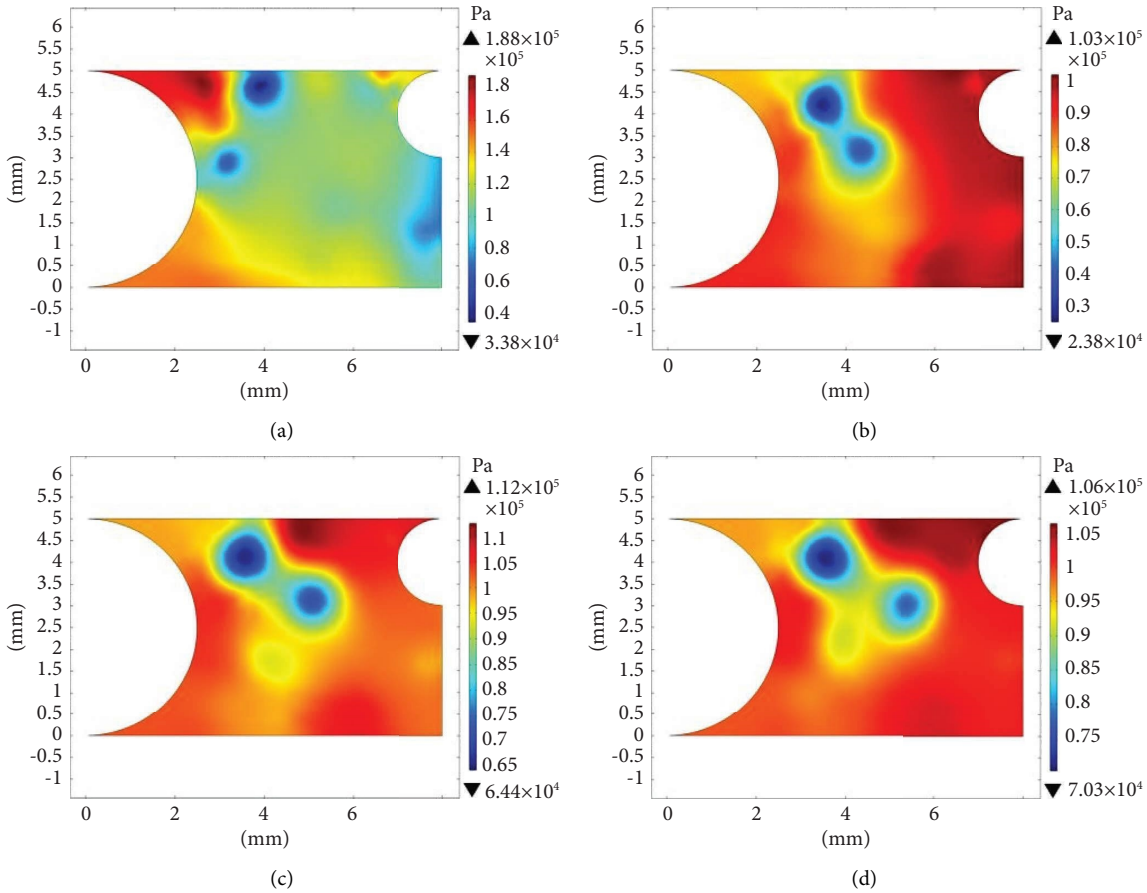

FIGURE 12: Pressure distribution cloud charts of 30%/70% CF_3I/CO_2 under 4 kA lightning impulse current at different times. (a) 4 μs. (b) 8 μs. (c) 12 μs. (d) 16 μs.

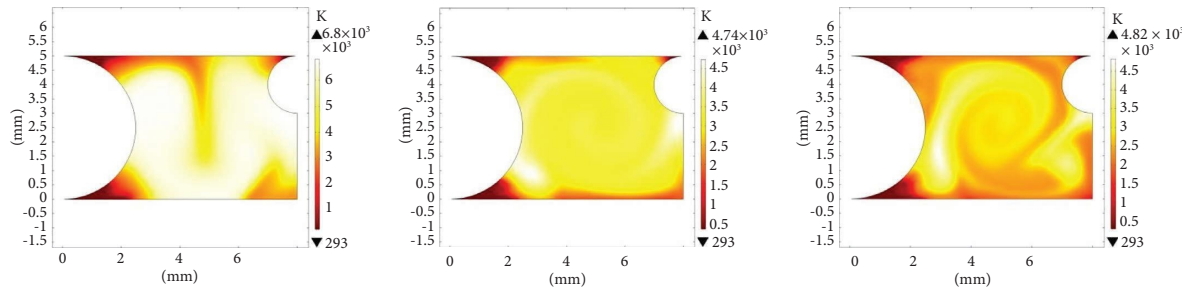

FIGURE 13: Temperature distribution cloud charts of different gases under 4 kA lightning impulse current at $t = 88\ \mu s$. (a) CO_2. (b) 10%/90% CF_3I/CO_2. (c) 30%/70% CF_3I/CO_2.

5. Conclusions

The arc magnetohydrodynamic model in a multipipe arc-quenching chamber is created using the finite element simulation program COMSOL. The simulation and analysis of the arc initiation in CO_2, 10%/90% CF_3I/CO_2, and 30%/70% CF_3I/CO_2 under lightning impulse current yields the following conclusions:

(1) The conductivity of the 30%/70% and 10%/90% CF_3I/CO_2 gas mixtures is lower than that of pure CO_2 during the arc formation period. The conductivity decreases as the amount of CF_3I in the gas mixture increases, indicating that the CF3I gas can more effectively prevent the formation of arcs.

(2) From the airflow velocity, the maximum airflow velocities of pure CO_2, 10%/90% CF_3I/CO_2, and 30% 70% CF_3I/CO_2 mixture are 1744 m/s, 1593 m/s, and 1840 m/s, respectively. With the increase in the proportion of CF_3I in the gas mixture, the airflow velocity increases, which is more beneficial to arc extinguishing.

(3) From a press perspective, according to the theory of arc explosion waves, when an arc is generated in a multipipe structure, more energy is accumulated within the structure, and the pressure generated also increases. The airflow speed will also be higher at the beginning, which plays a crucial role in extinguishing the arc. According to the press cloud map, the duration of overpressure generated by the mixed gas under lightning impulse current is longer than that of the pure CO_2 gas. The speed and pressure of the airflow during the generation of an arc are key factors in whether the arc can be quickly extinguished.

(4) From the pressure point of view, the duration of overpressure generated by the gas mixture under lightning impulse current is longer compared to that of the pure CO_2 gas.

(5) From the temperature of the last moments of the simulation, 30%/70% CF_3I/CO_2 is lower than CO_2, which proves that the temperature of 30%/70% CF_3I/CO_2 gas mixture decreases faster and the arc is quenched earlier.

Data Availability

The data that support the findings of this study are available from the corresponding author upon reasonable request.

Conflicts of Interest

The authors declare that they have no conflicts of interest regarding the publication of this paper.

Acknowledgments

This research was supported by the Guangxi Natural Science Foundation (2022GXNSFBA035613).

References

[1] L. G. Christophorou, J. K. Oltho, and R. Van Brunt, "Sulfur hexafluoride and the electric power industry," *IEEE Electrical Insulation Magazine*, vol. 13, no. 5, pp. 20–24, 1997.

[2] M. Taki, "Interruption capability of CF_3I gas as a substitution candidate for SF_6 gas," *IEEE Transactions on Dielectrics and Electrical Insulation*, vol. 14, 2007.

[3] L. Yi, H. Deng Hui, and G. H. Liu, "Analysis of carbon data related issues in the context of carbon peak and carbon neutral," *Science and Technology China*, vol. 4, pp. 11–14, 2021.

[4] B. Chervy, H. Riad, and A. Gleizes, "Calculation of the interruption capability of SF_6-CF_4 andSF_6-C_2F_6 mixtures. I. plasma properties," *IEEE Transactions on Plasma Science*, vol. 24, no. 1, pp. 198–209, 1996.

[5] Y. Kieffel, T. Irwin, P. Ponchon, and J. Owens, "Green gas to replace SF_6 in electrical grids," *IEEE Power and Energy Magazine*, vol. 14, no. 2, pp. 32–39, 2016.

[6] P. Widger, A. Haddad, and H. Griffiths, "Breakdown performance of vacuum circuit breakers using alternative CF_3I-CO_2 insulation gas mixture," *IEEE Transactions on Dielectrics and Electrical Insulation*, vol. 23, no. 1, pp. 14–21, 2016.

[7] H. Kasuya, Y. Kawamura, H. Mizoguchi, Y. Nakamura, S. Yanabu, and N. Nagasaki, "Interruption capability and decomposed gas density of CF_3I asa substitute for SF6 gas," *IEEE Transactions on Dielectrics and Electrical Insulation*, vol. 17, no. 4, pp. 1196–1203, 2010.

[8] M. Koch and C. M. Franck, "Partial discharges and breakdown in C_3F_8," *Journal of Physics D Applied Physics*, vol. 47, no. 40, Article ID 405203, 2014.

[9] Y. K. Deng and D. M. Xiao, "The effective ionization coefficients and electron drift velocities in gas mixtures of CF_3I

with N_2 and CO_2 obtained from boltzmann equation analysis," *Chinese Physics B: English version*, vol. 22, no. 3, p. 6, 2013.

[10] Y. Deng and D. Xiao, "Analysis of the insulation characteristics of CF_3I gas mixtures with Ar, Xe, He, N2, and CO_2 using Boltzmann equation method," *Japanese Journal of Applied Physics*, vol. 53, no. 9, Article ID 96201, 2014.

[11] Z. Hu, Z. Hui, and Q. Lin, "Study on lightning shock insulation characteristics of CF_3I-CO_2 mixture gas in extremely uneven electric field," *Insulation Materials*, vol. 25, no. 5, pp. 40–44, 2019.

[12] H. Katagiri, H. Kasuya, H. Mizoguchi, and S. Yanabu, "Investigation of the performance of CF_3I gas as a possible substitute for SF6," *IEEE Transactions on Dielectrics and Electrical Insulation*, vol. 15, no. 5, pp. 1424–1429, 2008.

[13] L. Chen, P. Widger, M. S. Kamarudin, H. Griffiths, and A. Haddad, "CF_3I gas mixtures: breakdown characteristics and potential for electrical insulation," *IEEE Transactions on Power Delivery*, vol. 32, no. 2, pp. 1089–1097, 2017.

[14] X. Zhang, J. Zhou, and J. Tang, "Experimental study on partial discharge characteristics of CF_3I/N_2 mixture gas," *High Voltage technology*, vol. 39, no. 2, pp. 287–293, 2013.

[15] J. D. E. Urquijo, A. M. Juárez, E. Basurto, and J. L. Hernández-Ávila, "Electron impact ionization and attachment, drift velocities and longitudinal diffusion in CF3I and CF_3I–N_2 mixtures," *Journal of Physics D Applied Physics*, vol. 40, no. 7, pp. 2205–2209, 2007.

[16] M. Habibi, "Study of shock wave and magnetic pressure effects on the rail gap switch surface used at the APF plasma focus device," *Journal of Fusion Energy*, vol. 30, no. 2, pp. 133–136, 2011.

[17] Y. Liu, Y. Zhao, and Y. Ren, "Analysis on the development process of arc channel for underwater high current pulsed discharge," *Transactions of China Electrotechnical Society*, vol. 36, no. 16, pp. 3525–3534, 2021.

[18] S. Liu, Y. Liu, Y. Ren, F. C. Lin, and Y. Liu, "Characteristic analysis of plasma channel and shock wave in electrohydraulic pulsed discharge," *Physics of Plasmas*, vol. 26, no. 9, Article ID 93509, 2019.

[19] J. Guo and L. Dai Hongyu, "Influence of arcing atmosphere on shock wave overpressure peak of high current pulsed arc," *Journal of Nanchang University*, vol. 46, no. 2, pp. 130–135, 2022.

[20] X. Gong, H. Shen, and H. Dai, "Peak value of shock wave overpressure and influencing factors of high-current pulse src," *High Voltage Engineering*, vol. 47, no. 12, pp. 4412–4419, 2021.

[21] J. M. Xiong, L. Li, H. Y. Dai, H. Wu, M. Peng, and F. Lin, "The development of shock wave overpressure driven by channel expansion of high current impulse discharge arc," *Physics of Plasmas*, vol. 25, no. 3, Article ID 32115, 2018.

[22] L. Z. Schlitz, S. V. Garimella, and S. H. Chan, "Gas dynamics and electromagnetic processes in high-current arc plasmas. Part I. model formulation and steady-state solutions," *Journal of Applied Physics*, vol. 85, no. 5, pp. 2540–2546, 1999.

[23] P. Freton, J. Gonzalez, and A. Gleizes, "Comparison between a two- and a three-dimensional arc plasma configuration," *Journal of Physics D Applied Physics*, vol. 33, no. 19, pp. 2442–2452, 2000.

[24] Y. Cressault, V. Connord, H. Hingana, P. Teulet, and A. Gleizes, "Transport properties of CF_3I thermal plasmas mixed with CO_2, air or N_2 as an alternative to SF_6 plasmas in high-voltage circuit breakers," *Journal of Physics D Applied Physics*, vol. 44, no. 49, Article ID 495202, 2011.